



PERGAMON

Deep-Sea Research II 49 (2002) 2649–2668

DEEP-SEA RESEARCH
PART II

www.elsevier.com/locate/dsr2

Controls on new production: the role of iron and physical processes

Anthony K. Aufdenkampe*, James W. Murray

School of Oceanography, University of Washington, Box 355451, Seattle, WA 98195, USA

Received 28 March 2001; received in revised form 4 September 2001; accepted 27 September 2001

Abstract

A coupled nitrogen–iron model is developed from simple mass balance equations to address fundamental controls on new production (NP) and how they relate to nitrate concentrations in high-nitrate-low-chlorophyll environments such as the central and eastern equatorial Pacific. The model demonstrates that a wide range of relationships between NP and mixed-layer nitrate is possible due to partial decoupling of nitrogen and iron cycles in the upper ocean. The shapes and slopes of these relationships are determined by the mode of physical forcing that introduces the most variability to the iron supply for a set of observations. When variability of upwelling fluxes is dominantly determined by changes in nutricline depth over changes in upwelling velocity, NP is a linear function of mixed-layer nitrate; whereas when variability in upwelling velocity dominates, NP takes on a hyperbolic function of nitrate. Fluctuations in atmospheric iron supply also introduce distinct patterns between NP and mixed-layer nitrate concentrations. Variability in nitrogen-to-iron ratios in exported organic matter, however, are not likely to drive large changes in NP or nitrate because of expected covariation with N:Fe ratios in upwelled source waters.

Within surface waters of the equatorial Pacific, variability in physical forcing exists over a wide range of temporal and spatial scales. Tropical instability waves, equatorially trapped internal gravity waves and daily fluctuations in zonal winds all predominantly drive short-term variability in upwelling velocities with minor changes to nutricline depth. El Niño cycles and Kelvin waves produce longer-term variability in nutricline depth with minimal changes in upwelling velocities. Comparisons of observed NP-to-nitrate relationships for individual cruises to the observed modes of physical forcing match model predictions quite well, with Zonal Flux and Flupac serving as end-member examples of these processes. These results support those from statistical studies (Aufdenkampe et al., *Deep-Sea Research* (2002) 2619–2648, Aufdenkampe et al., *Global Biogeochemical Cycles* 15 (2002) 101–113), by offering a mechanistic explanation for observations that the relationship between NP and nitrate is more variable between cruises than within cruises. © 2002 Elsevier Science Ltd. All rights reserved.

1. Introduction

New production (NP)—the portion of primary production (PP) stimulated by new nutrient inputs—provides a central framework for oceanographers studying upper-ocean biogeochemical cycles. Classically defined in terms of nitrogen (Dugdale and Goering, 1967), the concept of NP

*Corresponding author. Now at: Stroud Water Research Center, 970 Spencer Road, Avondale, PA 19311, USA. Tel.: +1-610-268-2153; fax: +1-610-268-0490.

E-mail address: aufdenkampe@stroudcenter.org (A.K. Aufdenkampe).

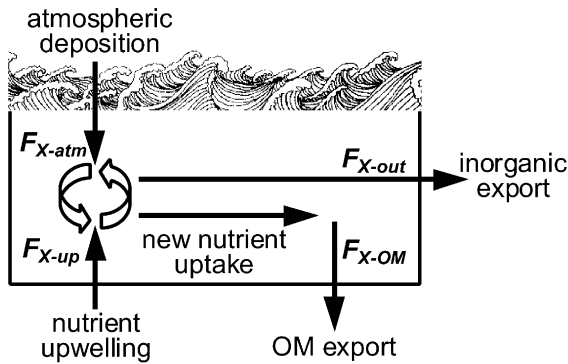


Fig. 1. Schematic of fluxes for a nutrient, X , into and out of the upper ocean "box." In a quasi-steady state ocean, where inventories of X do not change substantially over the time scale of interest, new production is equal to organic matter (OM) export or to the sum of inorganic inputs minus exports.

can easily be generalized to all bioactive elements. By considering mass balance requirements as per Eppley and Peterson (1979), the gross fluxes of bioactive elements through the euphotic zone thus become linked, in one way or another, by their rates and ratios of new biological uptake. Over the long term or in steady state, the balance of inorganic import fluxes for a nutrient minus its inorganic export must equal its net biological uptake within a given region, which in turn must translate to an export flux as dissolved and particulate organic matter (Fig. 1). Where one nutrient is limiting, and its inorganic export flux negligible, the supply rate of that limiting nutrient into the euphotic zone ultimately controls new production and the organic export fluxes of all bioactive elements.

New production has historically been defined in terms of nitrogen, largely due to the ease of distinguishing and measuring new versus regenerated forms and their respective uptake rates but also largely because nitrogen has been considered as limiting in many regions of the ocean. With the ubiquity of nitrate data, many studies have thus investigated relationships between new production and nitrate concentrations (Platt and Harrison, 1985; Dugdale and Wilkerson, 1992; McCarthy et al., 1999). However, in high-nitrate-low-chlorophyll (HNLC) waters such as the equatorial

Pacific, iron is now well established as the primary limiting nutrient (Martin and Fitzwater, 1988; Martin et al., 1994; Behrenfeld et al., 1996). For these regions the supply rate of iron to the upper ocean should control new production fluxes, yet iron concentration data are sparse and direct comparisons of iron flux estimates with measured new production have been limited to average values (Gordon et al., 1997; Landry et al., 1997). Therefore, even in HNLC environments, investigations of new production variability have generally relied on comparisons to other biological and chemical properties that might serve as proxies for the underlying controlling fluxes.

Recent multivariate statistical analyses of data from nine cruises measuring new production in the tropical Pacific (Aufdenkampe et al., 2001, 2002) has demonstrated that variability in new production is related largely to three main properties, PP (or chlorophyll), ammonium, and nitrate. The ability of multiple linear regression (MLR) to estimate new production in iron-limited ecosystems may result in some way from these properties acting as proxies for iron processes in the euphotic zone. For instance, the most important source of iron to the equatorial Pacific—water upwelled from the Equatorial Undercurrent (EUC)—is also the principle source of nitrate to the system (Toggweiler and Carson, 1995; Coale et al., 1996). Iron is thought to recycle in the upper water column at about the same rate as ammonium (Landry et al., 1997). Lastly, total iron inventory in the euphotic zone likely places an upper limit on primary productivity (Friedrichs and Hofmann, 2001) due to decreasing specific growth rates of phytoplankton as they get stretched for iron and approach maximum cellular C:Fe ratios (Sunda and Huntsman, 1995). Thus nitrate, ammonium, and PP (or Chl a) are indeed likely proxies for iron supply, recycling, and inventory, respectively. However, of these three the iron supply rate should be most strongly related to new production, yet nitrate is the weakest variable in the MLR of all nine cruises together. Then again, the new production to nitrate relationship is much stronger within individual cruises, with the slopes of these

relationships exhibiting substantial variability between cruises. What might cause this variable response to nitrate?

Although most iron enters the upper equatorial Pacific Ocean via upwelling, appreciable quantities of available iron—on average 5–30% of the total—are introduced via atmospheric deposition (Duce and Tindale, 1991; Gordon et al., 1997; Fung et al., 2000). This balance makes the equatorial Pacific relatively unique. For most of the world's oceans, including the north Pacific and much of the Southern Ocean, the aeolian iron source is a factor of 3–35 greater than the upwelling/mixing source (Fung et al., 2000) and rates of nitrate and iron supply are therefore largely uncoupled. In the equatorial Pacific however, the slight dominance of upwelled iron to total supply. The goal of this paper is thus to explore how variability in the coupling and decoupling of nitrogen and iron supply might reveal itself in

nitrate to new production relationships. Simple euphotic zone mass balances for nitrogen and iron are combined into a simple mechanistic model to gain insight into the biogeochemical and physical controls on new production and mixed-layer nitrate concentrations in the equatorial Pacific Ocean. Model results are then compared to data from six cruises to better understand patterns of observed new production variability. Finally, the implications of results are conceptually extended to other iron-limited regions of the world's oceans.

2. Model development

2.1. Coupling iron and nitrogen mass balance

The starting points in this examination are mass balance equations for nitrogen and iron for a

Table 1
Definitions and units for terms used in Fig. 1 and Eqs. (1)–(11)

Symbol	Units	Definition
[X]	$\mu\text{M} = \text{mmol m}^{-3}$	Average concentration of species X in the surface ocean “box”
D	m	Depth of the surface ocean box
[X] _{up}	mmol m^{-3}	Concentration of species X near the lower boundary of the box
[X] _{out}	mmol m^{-3}	Concentration of species X in the upper portion of the box
$F_{X\text{-atm}}$	$\text{mmol X m}^{-2} \text{d}^{-1}$	Atmospheric deposition flux of species X per unit ocean area
$F_{X\text{-up}}$	$\text{mmol X m}^{-2} \text{d}^{-1}$	Upwelling and vertical mixing flux of species X into the surface ocean box per unit ocean area
$F_{X\text{-OM}}$	$\text{mmol X m}^{-2} \text{d}^{-1}$	Organic matter export flux of species X per unit ocean area
$F_{X\text{-out}}$	$\text{mmol X m}^{-2} \text{d}^{-1}$	Inorganic advective export flux of species X per unit ocean area
(N/Fe)	mol mol^{-1}	Molar ratio of nitrogen-to-iron in upwelled waters or in organic matter
w	m d^{-1}	Upwelling velocity of water into the surface ocean box

Table 2
The assigned and observed ranges of parameters used in Fig. 1

Parameter	Assigned value	Observed range	Notes and references
$F_{\text{Fe-out}}$	0	~0	Surface [Fe] is generally below the detection limit in the upper tropical Pacific
$F_{\text{N-atm}}$	0	~0.005	(Gordon et al., 1997)
$F_{\text{Fe-atm}}$	10×10^{-6}	$2\text{--}25 \times 10^{-6}$	From average annual estimates (Duce and Tindale, 1991; Fung et al., 2000)
[NO ₃] _{out}	Variable	0–10	Assumed for simplicity to be the average concentration from 0 to 60 m
[NO ₃] _{up}	Variable	1–12	A flux weighted concentration, assumed to be that near 100–110 m
(N/Fe) _{up}	125,000	73,000–144,000	At 125 m (Johnson et al., 1997; http://color.mlml.calstate.edu/www/data/)
		125,000–280,000	At 80 m (Johnson et al., 1997; http://color.mlml.calstate.edu/www/data/)
(N/Fe) _{OM}	30,000	4,500–60,000	From laboratory experiments (Sunda and Huntsman, 1995)
		12,000–100,000	From oceanic regressions (Sunda, 1997)

simple, one-box euphotic zone (Fig. 1, Tables 1 and 2).

$$\frac{d(\text{area} \cdot \text{depth} \cdot [\text{N}])}{dt} = \text{area}(F_{\text{N-up}} + F_{\text{N-atm}} - F_{\text{N-OM}} - F_{\text{N-out}}), \quad (1)$$

$$\frac{d(\text{area} \cdot \text{depth} \cdot [\text{Fe}])}{dt} = \text{area}(F_{\text{Fe-up}} + F_{\text{Fe-atm}} - F_{\text{Fe-OM}} - F_{\text{Fe-out}}), \quad (2)$$

The rate of change in the inventory, $d(\text{volume} \cdot [\text{X}])/dt$, of a nutrient is equal to the surface area of ocean considered times the sum of its areal upwelling and vertical mixing fluxes ($F_{\text{X-up}}$) and atmospheric fluxes ($F_{\text{X-atm}}$) minus the sum of its total organic matter export fluxes ($F_{\text{X-OM}}$) and horizontal advective fluxes of any remaining dissolved nutrient species out of the box (i.e. in surface water) ($F_{\text{X-out}}$). Initially, both dissolved and particulate species are considered for these fluxes and atmospheric fluxes include gas exchange, fixation and deposition. These equations can be simplified by considering a one-dimensional box, dropping *area* from the equations, and by fixing the depth of the box to a constant value that is time-invariant.

A number of other simplifications are appropriate. The primary assumption is that iron is a limiting nutrient for all systems discussed below. This is supported by a growing consensus that iron limitation typically dominates equatorial Pacific ecosystems (Martin and Fitzwater, 1988; Martin et al., 1994; Behrenfeld et al., 1996; Landry et al., 1997). Furthermore, in the upper 80 m of the central and western equatorial Pacific dissolved iron concentrations are uniformly depleted to below the detection limit (Gordon et al., 1997) and to at least a factor of 2–3 less than the half-saturation constant for phytoplankton (Fitzwater et al., 1996). Therefore, because all iron introduced to the system appears to be taken up by the planktonic community, $F_{\text{Fe-out}}$ is assumed to be zero. Likewise, average atmospheric deposition of fixed nitrogen is 3–4 orders of magnitude less than upwelling fluxes (Gordon et al., 1997), and nitrogen fixation is likely negligible near the equator due to reasonably high turbulence by

winds and to short residence times of water near the surface (Carpenter and Capone, 1992). Therefore $F_{\text{N-atm}}$ is assumed to be zero. Lastly, because vertical advection generally dominates over vertical turbulent transport in the equatorial Pacific (Carr et al., 1995), upwelling is considered here as the primary driver of upward nutrient fluxes, $F_{\text{X-up}}$ (more in discussion). Furthermore, this model does not need to be strictly conceived as requiring vertical inputs. In highly stratified regions with weaker vertical exchange (e.g. off the equator), $F_{\text{X-up}}$ also can be thought of as resulting from horizontal advection (more in discussion).

Because euphotic zone inventories can be considered in quasi-steady state when integrated over long periods or when changes in inventory are small relative to changes in fluxes, $d[\text{X}]/dt = 0$. Thus, Eqs. (1) and (2) can each be solved for $F_{\text{N-OM}}$ and $F_{\text{Fe-OM}}$, respectively, and combined to arrive at

$$F_{\text{N-up}} - F_{\text{N-out}} = \frac{F_{\text{N-OM}}}{F_{\text{Fe-OM}}}(F_{\text{Fe-up}} + F_{\text{Fe-atm}}). \quad (3)$$

The resulting expression states that nitrate uptake rates (the difference between upwelling and inorganic export fluxes) is equivalent to iron fluxes into the euphotic zone when converted to biomass with the $(\text{N/Fe})_{\text{OM}}$ ratio of exported organic matter. In other words, new production in terms of nitrogen is equivalent to new production in terms of iron.

The simple assumption is made that upwelling fluxes are equal to the concentration of the nutrient at the bottom of the euphotic zone ($[\text{X}]_{\text{up}}$) times the vertical water volume flux at that boundary. In a one-dimensional model where the box is implied to be a 1 m^2 column, this water volume flux is equivalent to volume transport ($\text{m}^3 \text{ d}^{-1}$) per area (m^2), which translates directly into an upwelling velocity w (m d^{-1}). Thus $F_{\text{X-up}} = [\text{X}]_{\text{up}} * w$. Because the same amount of water comes in the bottom of the box as goes out the sides of the box, the horizontal export of mixed-layer nitrate ($F_{\text{N-out}}$) is likewise equivalent to the concentration within the box, $[\text{NO}_3^-]_{\text{out}}$, multiplied by the same water volume flux, w . Whereas w represents a physically meaningful

velocity of water into the 1 m^2 base of the box, the export water flux occurs over a much larger area and w does not represent an actual water velocity out of the box. Lastly, $F_{\text{N-up}}$ can be converted to an upwelling iron flux with the ratio of dissolved nitrogen-to-iron in the upwelled source waters, $(\text{N}/\text{Fe})_{\text{up}}$. Thus, Eq. (3) can be rearranged to get

$$[\text{NO}_3^-]_{\text{out}} w = \left(\frac{\text{N}}{\text{Fe}} \right)_{\text{up}} [\text{Fe}]_{\text{up}} w - \left(\frac{\text{N}}{\text{Fe}} \right)_{\text{OM}} ([\text{Fe}]_{\text{up}} w + F_{\text{Fe-atm}}). \quad (4)$$

This equation states that the horizontal export of mixed-layer nitrate is equal to the difference between the nitrate upwelling flux and the rate of nitrate uptake by plankton as a result of iron-stimulated new production.

2.2. Controls on mixed-layer nitrate

Dividing both sides by w and rearranging gives the average euphotic zone nitrate concentration as a function of upwelled dissolved iron concentration and atmospheric iron flux modulated by upwelling velocity, both converted to nitrogen.

$$[\text{NO}_3^-]_{\text{out}} = [\text{Fe}]_{\text{up}} \left(\left(\frac{\text{N}}{\text{Fe}} \right)_{\text{up}} - \left(\frac{\text{N}}{\text{Fe}} \right)_{\text{OM}} \right) - \frac{1}{w} F_{\text{Fe-atm}} \left(\frac{\text{N}}{\text{Fe}} \right)_{\text{OM}}. \quad (5)$$

This expression gives significant insight into the equatorial system, once each of the terms is placed into context. Conceptually extrapolating to a system more realistic than the one-box euphotic zone, one realizes that because both $[\text{NO}_3^-]$ and w (and thus divergent export) vary with depth, the concentration of mixed-layer nitrate, $[\text{NO}_3^-]_{\text{out}}$, represents a flux weighted export concentration. Conveniently, mean vertical velocity profiles on the equator suggest that Ekman divergence results in relatively uniform horizontal advection out of the upper 60 m (Brady and Bryden, 1987; Halpern and Freitag, 1987), whereas below 60 m advection is increasingly convergent with depth. Therefore, $[\text{NO}_3^-]_{\text{out}}$ can be thought of as the 0–60 m depth-averaged concentration. Likewise, $[\text{NO}_3^-]_{\text{up}}$ and $[\text{Fe}]_{\text{up}}$ must represent a flux-weighted mean.

Greater than half of water fluxes enter the euphotic zone from 125 m, with most of the remainder by 80 m (Brady and Bryden, 1987; Halpern and Freitag, 1987). Therefore, for simplicity $[\text{NO}_3^-]_{\text{up}}$ and $[\text{Fe}]_{\text{up}}$ can be thought of as concentrations near 100–110 m.

The ratio of nitrate to dissolved iron in upwelled source waters is surprisingly constant. For the six stations in which dissolved iron profiles have been measured at the equator (during Feline, EqPac TS I and TS II and PlumEx Sta. 8–10; Johnson et al., 1997, Appendix A and <http://color.mlml.calstate.edu/www/data/>), N:Fe ratios increase from the core of the EUC with ratios of 60,000–70,000 to a mean ratio at 125 m of $116,000 \pm 26,000$ and $199,000 \pm 58,000$ at 80 m. Again, the nitrate-to-iron ratio upwelled to the euphotic zone, $(\text{N}/\text{Fe})_{\text{up}}$, should correspond to a ratio of fluxes or at least a ratio of flux-weighted $[\text{NO}_3^-]_{\text{up}}$ and $[\text{Fe}]_{\text{up}}$ values. Gordon et al. (1997) used a one-dimensional advection–diffusion model to calculate mean nitrate and iron fluxes from the same data employed here. Their value for $(\text{N}/\text{Fe})_{\text{up}}$ of 125,000 is thus reasonable for this discussion for all equatorial stations.

Nitrogen-to-iron ratios in exported organic matter are more difficult to constrain. Diatoms in the laboratory take up nitrate and iron in molar ratios ranging from 4,500 to 60,000 (Sunda and Huntsman, 1995), and ratios determined by regressions of dissolved Fe to apparent oxygen utilization (AOU) in a wide range of oceanic environments yielded N:Fe regeneration ratios of 12,000–100,000 (Sunda, 1997). For both data sets, phytoplankton ratios were a strong function of iron limitation, with conditions typical of the equatorial Pacific giving values consistently in the higher end of each range. Actual ratios in exported organic matter are even more difficult to constrain than these uptake ratios, and values depend on whether dissolved or particulate organic matter is considered because dissolved iron is strongly scavenged onto particles (Johnson et al., 1997). During EqPac TS I and TS II, molar ratios of dissolved organic nitrogen to total dissolved iron were $>250,000$ in most of the euphotic zone, where dissolved iron was below the detection limit (nitrogen from H. Ducklow <http://usjgofs.whoi>).

edu/jg/dir/jgofs/, assuming a C/N = ~ 8 as per Libby and Wheeler (1997), and iron data from Johnson et al., 1997, Appendix A). On the other hand, ratios of suspended particulate organic nitrogen to suspended particulate iron were 6500–9000 in the upper 40 m and decreased with depth to ~ 400 below 150 m (data from H. Ducklow <http://usjgofs.whoi.edu/jg/dir/jgofs/> and Johnson et al., 1997, Appendix A). Although no direct ratio estimates exist for larger sinking particles (i.e. from traps), one might expect N:Fe ratios to be even lower because of enhanced scavenging efficiency due to a smaller diffusional boundary layer around the particle as it sinks. For instance, carbon-to- ^{234}Th ratios are known to be smaller on larger actively sinking particle versus smaller suspended particles (Murray et al., 1996). Given that sinking particles likely account for more than half of the organic matter export in the equatorial Pacific (Archer et al., 1997; Hansell et al., 1997a, b; Zhang and Quay, 1997) but that the actual balance between dissolved and particulate export and associated N:Fe ratios is largely unconstrained, it appears most reasonable to base $(\text{N}/\text{Fe})_{\text{OM}}$ on values in the lower range of uptake ratio estimates. Therefore, we initially assume $(\text{N}/\text{Fe})_{\text{OM}}$ as having somewhat variable values centered around 30,000, as assumed by Johnson et al. (1997) and in the middle of the range used by Leonard et al. (1999) (more below).

Average atmospheric dust fluxes of available iron to the equatorial Pacific near 140°W have recently been estimated to be $1.8\text{--}18 \text{ nmol Fe}_{\text{dis}} \text{ m}^{-2} \text{ d}^{-1}$ (Fung et al., 2000). This agrees well with the estimate of $5\text{--}25 \text{ nmol Fe}_{\text{dis}} \text{ m}^{-2} \text{ d}^{-1}$ used in several previous studies (Coale et al., 1996; Gordon et al., 1997) based on the work of Duce and Tindale (1991). This close agreement is somewhat coincidental. Duce and Tindale (1991) found deposition in the equatorial Pacific of total Fe to be more than three times lower than Fung et al. (2000) yet they assumed 10–50% of it to be solubilized and bioavailable as opposed to 1–10% in the more recent study. These lower dust iron solubilities are supported by several studies (Spokes et al., 1994; Zhuang et al., 1995; Zhu et al., 1997), yet do not take into account evidence that particulate iron is substantially solubilized by

photolysis (Johnson et al., 1994) and during ingestion by mixotrophic phytoplankton (Maranger et al., 1998) and protozoan zooplankton (Barbeau et al., 1996; Barbeau and Moffett, 2000). Issues of bioavailability thus add considerable uncertainty to atmospheric iron flux estimates. Furthermore, these iron fluxes are derived from annual dust supply rates, yet temporal variability is likely to be quite high due to the variable nature of dust storm events and atmospheric circulation (Tegen and Miller, 1998). For instance, only a few 2–4 day events can account for more than half of annual deposition at locations in the Pacific (Duce and Tindale, 1991). For the purposes of simplicity for this discussion, we use an atmospheric iron flux value, $F_{\text{Fe-atm}}$, of $10 \text{ nmol Fe}_{\text{dis}} \text{ m}^{-2} \text{ d}^{-1}$, as done by Leonard et al. (1999). However, due to the highly episodic nature of dust deposition in the Pacific, the median daily deposition flux is likely to be much lower.

Thus, Eq. (5) states that mixed-layer nitrate concentrations depend primarily and perhaps equally on three properties that can vary in space and time (1) the nutrient concentration at the base of the euphotic zone (e.g. $[\text{Fe}]_{\text{up}}$), which is a function of the nutricline depth, (2) atmospheric iron fluxes ($F_{\text{Fe-atm}}$), and (3) the magnitude of Ekman divergent upwelling (w). Mixed-layer nitrate concentrations are further modulated by changes in the nitrogen-to-iron ratios in upwelled waters and exported organic matter.

2.3. The relation of mixed-layer nitrate to new production

To get new production, NP, as a function of $[\text{NO}_3^-]_{\text{out}}$ Eq. (5) is multiplied by wB (B defined in Eq. (8)) then A (defined in Eq. (7)) is added to both sides. Recognizing that new production equals the right-hand side of Eq. (3):

$$\text{NP} = A + wB[\text{NO}_3^-]_{\text{out}}, \quad (6)$$

where

$$A = \left(\frac{\text{N}}{\text{Fe}} \right)_{\text{OM}} F_{\text{Fe-atm}} (1 + B) \quad (7)$$

and

$$B = \frac{(N/Fe_{OM})}{(N/Fe_{up}) - (N/Fe_{OM})}. \quad (8)$$

The mass balance Eqs. (1) and (2) now yield a form that is directly comparable with results from MLR studies. However, Eq. (6) is less straightforward to interpret than it first appears, because $[NO_3^-]_{out}$ is a function of both w and nutricline depth (i.e. $[NO_3^-]_{up}$ or $[Fe]_{up}$) (see Eq. (5)). From the left-hand side of Eq. (3), we see that $NP = w * ([NO_3^-]_{up} - [NO_3^-]_{out})$. Equating the right-hand side of this expression to that of Eq. (6) and rearranging gives another form of Eq. (5).

$$[NO_3^-]_{out} = \frac{[NO_3^-]_{up} - A/w}{1 + B}. \quad (9)$$

Thus, to understand the functionality of NP with respect to surface nitrate concentrations, $[NO_3^-]_{out}$, it is easiest to first consider the two special cases in which either w or $[NO_3^-]_{up}$ is held constant. For simplicity we also initially consider both N:Fe ratios and F_{Fe-atm} as constant.

From Eq. (6) it is clear that when w is constant, new production is a linear function of mixed-layer nitrate concentrations. In this special case, iron fluxes to the euphotic zone, $[NO_3^-]_{out}$ and NP all vary only as a function of changing nutricline (or thermocline) depth. The Y -intercept (A), which can be interpreted as the new production that would occur even at negligible concentrations of mixed-layer nitrate, is equal to atmospheric iron deposition times the nitrogen-to-iron ratio of exported organic matter plus an additional amount proportional to the ratio B . The term B represents the ratio of nitrate that potentially can be directly taken up in conjunction with upwelled iron to the “excess” nitrate that cannot be taken up with upwelled iron. Although combinations of all possible values of $(N/Fe)_{OM}$ or $(N/Fe)_{up}$ can yield B in the range of 0.05–2.0 ($B = 0.32$ for $(N/Fe)_{OM} = 30,000$ and $(N/Fe)_{up} = 125,000$), B may in fact be much more constant than either of the N:Fe ratios because of expected covariance between the two, especially within a single hydrographic regime.

It is also clear from Eq. (6) and (9) that NP is not linear with respect to $[NO_3^-]_{out}$ when w is not

constant between stations. In fact, when iron fluxes, $[NO_3^-]_{out}$ and NP all vary only as a function of upwelling velocity, and nutricline depth is thus assumed to be constant, this function becomes asymptotic. Substituting $w = NP / ([NO_3^-]_{up} - [NO_3^-]_{out})$ into Eq. (6), factoring out NP and rearranging gives the asymptotic form:

$$NP = \frac{A}{1 - B \left(\frac{[NO_3^-]_{out}}{[NO_3^-]_{up} - [NO_3^-]_{out}} \right)}. \quad (10)$$

Here the term $[NO_3^-]_{out} / ([NO_3^-]_{up} - [NO_3^-]_{out})$ represents the ratio of nitrate that is not taken up to the nitrate that is actually taken up. In cases where $F_{Fe-atm} \ll F_{Fe-up}$, then $A \ll NP$, leaving $1/B$ to approach the term, $[NO_3^-]_{out} / ([NO_3^-]_{up} - [NO_3^-]_{out})$. From this the vertical asymptote can be derived:

$$[NO_3^-]_{out} = \frac{[NO_3^-]_{up}}{1 + B}. \quad (11)$$

Conversely, the horizontal asymptote, when $[NO_3^-]_{out} \ll [NO_3^-]_{up}$ and atmospheric iron fluxes dominate, is given by new production equal to A , which is also the intercept of Eq. (6).

A visual summary of new production as a function of $[NO_3^-]_{out}$ under these two scenarios of physical forcing (constant w or constant $[NO_3^-]_{up}$) is plotted in Fig. 2a. Linear contours of constant upwelling velocity are plotted using Eq. (6), with $(N/Fe)_{up} = 125,000$, $(N/Fe)_{OM} = 30,000$ and $F_{Fe-atm} = 10 \text{ nmol Fe m}^{-2} \text{ d}^{-1}$. Similarly, the hyperbolic contours corresponding to conditions of constant source-water nutrient concentration, $[NO_3^-]_{up}$, are plotted according to Eq. (10).

Notice that the conditions for which $NP \approx A$ are diverse. When the nutricline is very deep and upwelled and subsequently surface nitrate concentrations are negligible, new production is determined by atmospheric iron fluxes even at high upwelling velocities (Eq. (6)). On the other hand, very low upwelling velocities can result in the same new production rates even when the thermocline is shallow and mixed-layer nitrate concentrations high. Eq. (9) proves to be very informative in these latter two cases. First, we see that $[NO_3^-]_{up}$ must remain greater than A/w for $[NO_3^-]_{out}$ to be positive. At concentrations below A/w , nitrogen becomes the limiting nutrient over iron. Likewise,

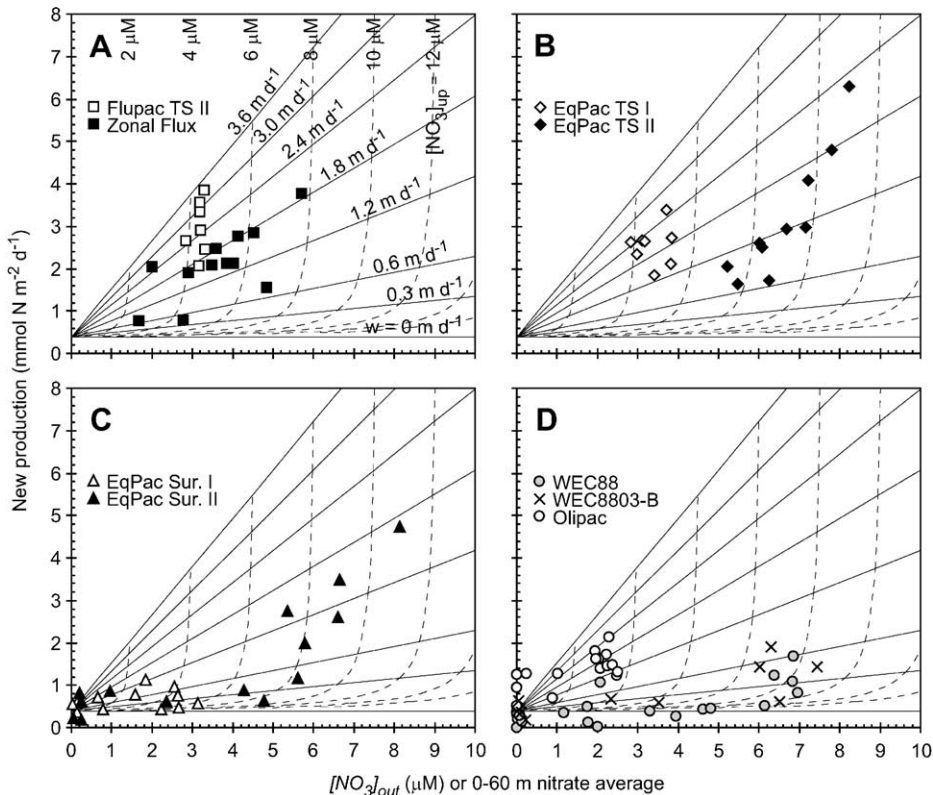


Fig. 2. Coupled nitrogen–iron mass balance model, in which new production is a function of average exported nitrate concentration ($[\text{NO}_3^-]_{\text{out}}$), average upwelled nitrate concentration ($[\text{NO}_3^-]_{\text{up}}$) and upwelling velocity (w), with atmospheric iron deposition ($F_{\text{Fe-atm}} = 10 \text{ nmol m}^{-2} \text{ d}^{-1}$), nitrogen:iron organic export ratios ($(\text{N}/\text{Fe})_{\text{OM}} = 30,000$), and dissolved nitrogen:iron upwelling ratios ($(\text{N}/\text{Fe})_{\text{up}} = 125,000$) taken at constant, representative values. Plots compare (A) model contours of $[\text{NO}_3^-]_{\text{up}}$ and w with observations from Zonal Flux and Flupac TS II (Aufdenkampe et al., in press, 2002), (B) EqPac Time Series I and II (nutrient and nitrate uptake data from P. Wheeler, <http://www1.who.edu/jgofs.html>), and (C) EqPac Surveys I and II (McCarthy et al., 1996, nutrient data from C. Garside, <http://www1.who.edu/jgofs.html>), and (D) WEC88, WEC8803-B and Olipac (Dugdale et al., 1992; Peña et al., 1992; Raimbault et al., 1999). Several Olipac points near the origin are obscured. Contours above $w = 3.6 \text{ m d}^{-1}$, which become increasingly closely spaced, have been removed to simplify presentation. Open symbols represent cruises during El Niño conditions.

the system ceases to be iron-limited where $w < A/[\text{NO}_3^-]_{\text{up}}$. Once nitrogen limitation predominates over iron limitation, we leave the bounds of our model assumptions and NP is no longer a function of the iron supply rate. However, it is logical that the iron supply rate continues to set an upper bound on new production (i.e. $\text{NP} < A$) even under conditions of nitrogen limitation. Furthermore, in cases where upwelling has stopped temporarily (i.e. on the equator near 170°W just prior to sampling during Flupac) (Rodier et al., 2000), the slow rate of drawdown of mixed-layer nitrate may be a direct function of atmospheric iron deposi-

tion, although our model would not apply because of our assumption of quasi-steady state.

2.4. Sensitivity of model to $F_{\text{Fe-atm}}$, $(\text{N}/\text{Fe})_{\text{up}}$ and $(\text{N}/\text{Fe})_{\text{OM}}$

In previous discussion of the model (Eqs. (6) and (10), Fig. 2), three of the five independent variables were assigned constant “average” values. Not only is it difficult to confidently assign average values for atmospheric iron supply and nitrogen-to-iron ratios in upwelled water and in exported organic matter, but actual values are likely to be

variable in space and time. How sensitive then are model results to poorly assigned values for these three parameters or to variation in these values?

2.4.1. Atmospheric iron deposition

Of these three parameters, variability in atmospheric iron deposition ($F_{\text{Fe-atm}}$) is perhaps the least constrained. Most of the year, dust supply in the equatorial Pacific is likely to be negligible, yet for a few scattered weeks deposition could be quite significant relative to upwelling fluxes. The main effect of an atmospheric iron pulse would be to uniformly shift all new production values up by a nearly constant amount (Fig. 3a–c). At the same time, mixed-layer nitrate inventories would decrease slightly, even if the nitrogen supply rate does not change. An atmospheric iron flux of

$1.0 \text{ nmol Fe m}^{-2} \text{ d}^{-1}$, which might be typical during normal conditions, reduces A (the intercept of Eq. (6) and asymptote of Eq. (10)) to nearly zero and tightens curves for constant $[\text{NO}_3^-]_{\text{up}}$ to nearly match their vertical asymptotes (Fig. 3b). Given no change in other conditions, an increase in atmospheric iron supply from 1 to 33 $\text{nmol Fe m}^{-2} \text{ d}^{-1}$ would result in all new production rates increasing by $\sim 1.3 \text{ mmol N m}^{-2} \text{ d}^{-1}$, similar to rates measured at some stations in oligotrophic waters during Flupac TS I (Rodier and Le Borgne, 1997) or at some Olipac stations (Raimbault et al., 1999). For higher dust supply, curves for constant $[\text{NO}_3^-]_{\text{up}}$ also rise to meet their asymptotes more gently, thus slightly reducing mixed-layer nitrate concentrations for a given upwelling velocity and nutricline depth.

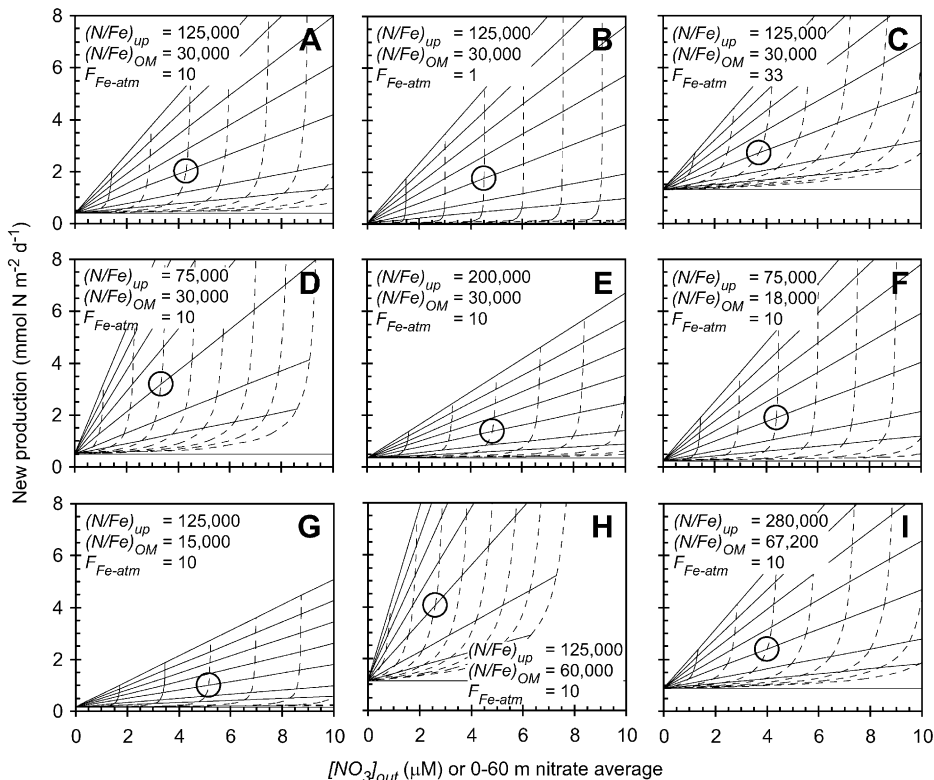


Fig. 3. Sensitivity of model results to assigned parameters. Plots compare (A) parameter values used in Fig. 2 and the first half of the discussion with: (B) lower and (C) higher rates of atmospheric iron deposition; (D) lower and (E) higher values for upwelled nitrate-to-iron ratios; and (G) lower and (H) higher values of nitrogen-to-iron ratios in exported organic matter. Plots (F) and (I) illustrate that likely covariation in both ratios substantially reduces model sensitivity. The point corresponding to 1.2 m d^{-1} upwelling velocity (w) and $6 \mu\text{M}$ upwelled nitrate concentrations ($[\text{NO}_3^-]_{\text{up}}$) is circled as a common reference to track changes in the new production to nitrate relationship when $(\text{N}/\text{Fe})_{\text{up}}$, $(\text{N}/\text{Fe})_{\text{OM}}$ or $F_{\text{Fe-atm}}$ are variable.

2.4.2. Nitrogen-to-iron ratios in upwelled waters

N:Fe ratios in upwelled source waters also have an effect on how upwelling rates and nitricline depth together determine new production and mixed-layer nitrate (Fig. 3a,d,e). A decrease in $(\text{N}/\text{Fe})_{\text{up}}$ to 75,000, a ratio close to those observed within the EUC, reduces the term B (Eq. (8)), thereby increasing the slope for contours for constant upwelling velocity and decreasing the asymptotic mixed-layer nitrate concentration that would be observed for a given upwelled concentration (Fig. 3d). An increase in $(\text{N}/\text{Fe})_{\text{up}}$ has the opposite effect (Fig. 3e); variability in upwelling velocities would translate to smaller changes in NP, and mixed-layer nitrate concentrations would be elevated. Because the term B has a small effect on the term A , variability in $(\text{N}/\text{Fe})_{\text{up}}$ would be positively correlated to minor fluctuations in minimum new production rates.

2.4.3. Nitrogen-to-iron ratios in exported organic matter

Ratios of nitrogen-to-iron in phytoplankton biomass are known to be highly variable (Sunda and Huntsman, 1995). By inference, N:Fe in exported organic matter are likely to show similar variability, although this ratio may be lower due to iron scavenging by organic particles (Johnson et al., 1997). Decreasing $(\text{N}/\text{Fe})_{\text{OM}}$ strongly decreases terms A (Eq. (7)) and B (Eq. (8)), thereby flattening contours for constant upwelling and increasing asymptotic values for contours of constant $[\text{NO}_3^-]_{\text{up}}$ (Fig. 3g). Increasing $(\text{N}/\text{Fe})_{\text{OM}}$ does the opposite to model contours (Fig. 3h). Furthermore, large changes in minimum NP values in these plots illustrate the importance of $(\text{N}/\text{Fe})_{\text{OM}}$ in modulating the efficiency in which atmospheric iron is exported as organic matter.

Variability in these three parameters— $F_{\text{Fe-atm}}$, $(\text{N}/\text{Fe})_{\text{up}}$ and $(\text{N}/\text{Fe})_{\text{OM}}$ —could all contribute to the pattern in new production and mixed-layer nitrate observed for a set of stations. Model results appear to be most sensitive to changes in the two iron ratios, and previous modeling studies have noted high sensitivity of primary productivity to changes in planktonic C:Fe ratios (Loukos et al., 1997; Leonard et al., 1999). However, $(\text{N}/\text{Fe})_{\text{up}}$ and $(\text{N}/\text{Fe})_{\text{OM}}$ are not likely to vary indepen-

dently. Sunda and Huntsman (1995) found, in laboratory cultures of an oceanic diatom, that by increasing ambient dissolved iron from 4 to 250 pM, biomass C:Fe ratios decreased by a factor of fourteen. Likewise, C:Fe ratios determined from regressing $[\text{Fe}]$ to AOU appear to be a strong function of iron inventories (Sunda, 1997). This covariation would thus substantially mitigate any sensitivity in the model to variability in nitrogen-to-iron ratios, due to the opposing effects of each variable on model contours (Eq. (8), Fig. 3d-e,g-h). The effect of covariation in $(\text{N}/\text{Fe})_{\text{up}}$ and $(\text{N}/\text{Fe})_{\text{OM}}$ can be seen by comparing reference model contours (Fig. 3a) with those resulting from decreasing both ratios (Fig. 3f) and from increasing both ratios (Fig. 3i). For all three of these plots, ratios were selected such that the term B (Eq. (8)) remained constant ($B = 0.316$) in order to highlight the additional effect of $(\text{N}/\text{Fe})_{\text{OM}}$ on the term A (Eq. (7)), yet it is clear from other plots that even loose covariation between the two N:Fe ratios will minimally affect model contours.

A large pulse of iron from an atmospheric deposition event, however, could trigger a decrease in $(\text{N}/\text{Fe})_{\text{OM}}$ without a concurrent decrease in $(\text{N}/\text{Fe})_{\text{up}}$. In such a scenario, lower values of $(\text{N}/\text{Fe})_{\text{OM}}$ would act to partially offset enhanced nitrate-uptake rates that would result from additional atmospheric iron supply (Fig. 3c,g). However, because atmospheric iron supply could conceivably increase by one to two orders of magnitude whereas $(\text{N}/\text{Fe})_{\text{OM}}$ is not likely to decrease by more than a factor of 5, it is likely that the positive effect of additional iron on nitrate uptake rates would dominate.

3. Discussion

The important result of these model equations—all derived from coupled nitrogen and iron mass balance—is that HOW the upwelling flux varies is the most important factor in determining the relationship between new production and mixed-layer nitrate for a set of stations. Because the areal upwelling flux is the product of upwelling velocity and the average concentration of the upwelled water, different modes of physical forcing that

drive these components differentially should have a profound effect on how new production and mixed-layer nitrate concentrations covary within a set of observations. This result is a consequence of the partial decoupling of nitrogen and iron fluxes by atmospheric iron deposition.

Direct biogeochemical and physical observations during six cruises to the region—Zonal Flux, Flupac, EqPac Time Series I and II, and EqPac Surveys I and II—offer much insight into the validity of the model by allowing the comparison of measured values of NP and $[\text{NO}_3^-]_{\text{out}}$ with independent observations of physical forcing (Table 3). Data overlaid over modeled contours of w and modeled contours of $[\text{NO}_3^-]_{\text{up}}$ appear at first glance to fit well within the range of model parameters chosen (Fig. 2). Individual stations plot near $[\text{NO}_3^-]_{\text{up}}$ contours with values matching those found in their lower euphotic zones. Likewise, the 1.2 and 1.8 m d^{-1} contours in w that pass through the middle of plotted stations also neatly coincide with the 1.2 and 2.0 m d^{-1} upwelling velocities at 120 and 90 m found in average profiles of w at the equator and 140°W (Brady and Bryden, 1987). This general comparison lends confidence that the numerous assumptions made to this point are generally valid. However, most striking is that

patterns of NP relative to mixed-layer nitrate suggest by comparison to model contours that physical forcing was quite different between cruises. Do independent observations of physical conditions during these cruises match those suggested by the model?

3.1. Variability in modes of physical forcing: comparing model to observation

Differences between stations in upwelling velocity and/or depth of nutricline result in changes to upwelling iron fluxes and thus new production. However, model results suggest that a difference in nutricline depth between stations is required to effect an observable change in upper euphotic zone nitrate inventories at all but the lowest upwelling rates. The new production to nitrate inventory relationship for a particular cruise thus depends on the type of temporal and/or spatial variability that is encountered during the cruise. In a simplistic, steady-state ocean, physical variability would be driven by the locations of stations within various hydrographic regions. A zonal transect along the equator for, instance, would sample stations with increasing $[\text{NO}_3^-]_{\text{up}}$ to the east; yet given a uniform wind field, upwelling velocities would remain

Table 3
Cruises and stations used to compare observation with model results

Cruise	Stations	Dates	Latitude	Longitude	References
WEC88	21	2/22/88–3/15/88	15°N–15°S	150°W	Dugdale et al. (1992), Wilkerson and Dugdale (1992)
WEC8803-B	13	3/31/88–4/23/88	15°N–15°S	133°W–143°W	Peña et al. (1992)
EqPac Survey I	12	2/3/92–3/7/92	12°N–12°S	135°W–140°W	McCarthy et al. (1996)
EqPac Time Series I	8	3/26/92–4/9/92	0°	140°W	Wheeler, US-JGOFS Home Page
EqPac Survey II	15	8/9/92–9/12/92	12°N–12°S	135°W–140°W	McCarthy et al. (1996)
EqPac Time Series II	10	10/2/92–10/20/92	0°	140°W	Wheeler, US-JGOFS Home Page
Flupac TS I	1	10/2/94–10/7/94	0°	167°E	Rodier and LeBorgne (1997), Navarette (1998)
Flupac TS II	7	10/19/94–10/25/94	0°	150°W	Navarette (1998), Aufdenkampe et al. (2002)
Olipac	19	11/6/94–11/29/94	1°N–16°S	150°W	Raimbault et al. (1999)
Zonal Flux	12	4/20/96–5/10/96	2°N–2°S	165°E–150°W	Aufdenkampe et al. (2002)

relatively constant. A meridional transect to the equator would show a mixed trend, as both w and $[\text{NO}_3^-]_{\text{up}}$ increase near the equator.

The reality of the equatorial Pacific region is that various physical processes force upper-ocean temporal and spatial variability with a large range of periods and characteristic wavelengths (Kessler and McPhaden, 1995). Tropical instability waves (TIW) can drive upwelling velocities to range as large as $+15$ to -10 m d^{-1} over a typical 20–30 day period and over distances of a few hundred kilometers (Harrison, 1996; Foley et al., 1997). These rapid changes in upwelling velocity profiles are not necessarily correlated with changes in depths of isotherms due to patterns of variable convergence and divergence with depth (Harrison, 1996). Equatorially trapped internal gravity waves (IGW) drive high frequency (6–8 day period) oscillations in vertical velocity (as large as $+10$ to -10 m d^{-1}) with minor fluctuations to thermocline depths due to the short period (Wunsch and Gill, 1976; Friedrichs and Hofmann, 2001). Such high-frequency variability is filtered out of many datasets, yet can have substantial influence in biological systems with short doubling times (1–2 days) (Friedrichs and Hofmann, 2001). On the other hand, Kelvin waves drive changes in thermocline depth as large as 10 m in a day, with a 40–70 day period and zonal wavelengths an order of magnitude larger than TIWs (Foley et al., 1997). On interannual time-scales, El Niño-La Niña cycles exhibit changes in thermocline depths of up to 100 m. Clearly, all of these physical processes offer substantial potential to drive upwelling fluxes quite differently, either via w , $[\text{NO}_3^-]_{\text{up}}$ or both. A time-series cruise that measured new production during strong TIW activity would find a different new production to nitrate relationship than a cruise sampling the passage of a Kelvin wave or during steadier conditions.

Let us now look in detail at how independent measurements and observations during each cruise match with model results. This comparison will allow confirmation of whether the model is generally valid and also will offer insight into why different patterns of NP and mixed-layer nitrate were observed during different cruises.

3.1.1. Zonal flux

This cruise in many ways sampled the idealized, steady-state equatorial Pacific described above. Nitrate concentrations at the bottom of the euphotic zone (80–120 m) increased gradually to the east from 4.5–6.5 μM at 170°E to 10–14 μM at 150°W. Upwelling velocities were also likely to have been quite uniform over the transect. Zonal easterly winds were nearly constant over the entire transect at $\sim 6.5 \text{ m s}^{-1}$, very near to the climatological mean (NOAA TAO web site, <http://www.pmel.noaa.gov/tao/>), and isotherm depths for the entire transect were very stable (constant with time) for the entire month of April 1996. Typical of this season, there was no evidence of TIW activity. These observations of physical conditions are quite in line with inferences from the nitrogen–iron model. New production observations made during Zonal Flux for the most part plot along a line of constant upwelling velocity of $\sim 1.8 \text{ m d}^{-1}$ and across increasing contours of upwelled nitrate, from ~ 4 to $\sim 8 \mu\text{M}$ (Fig. 2a). These values not only closely match the flux-weighted 60–120 m mean vertical velocity of $1.6\text{--}1.7 \text{ m d}^{-1}$ that can be calculated from climatological average velocity profiles for the region (Brady and Bryden, 1987; Halpern and Freitag, 1987) but also agree with observed concentrations at upwelling depths of 90–110 m (Aufdenkampe et al., 2002). Thus, the variability in nutrient fluxes sampled during Zonal Flux appear largely driven by changes in upwelled nitrate (and iron) concentrations as a result of changes in nutricline depth along the transect.

3.1.2. Flupac Time Series II at 150°W

Flupac TS II observed nearly the opposite type of forcing on nutrient fluxes than that observed during Zonal Flux. Nitrate concentrations at the bottom of the euphotic zone at 80 and 120 m showed exceedingly little variability, remaining near ~ 4.5 and $\sim 7.5 \mu\text{M}$, respectively. These values are much lower than those observed on the equator at similar longitude during Zonal Flux, EqPac TS I, TS II or Survey II, because the thermocline was significantly depressed after passage of a strong Kelvin wave (TAO web site and Eldin et al., 1997). However, upwelling velocities

appear to have exhibited the opposite extreme at 150°W during TS II.

One of the most interesting observations from Flupac was that near the sharp western boundary (at 172°W) of the HNLC area, the passage of a strong Kelvin wave appeared to have stopped upwelling fluxes of nutrients completely for the entire month prior to sampling (Eldin et al., 1997; Rodier et al., 2000). However, conditions at 150°W during TS II were quite different due to moderate TIW activity in the cold-tongue region (Eldin et al., 1997; Dunne et al., 2000) as is typical at that time of year. Meridional velocities (v) measured by the TAO buoy at 140°W show five distinct TIWs passed the buoy from August to November (Fig. 4). In particular, the southward (negative) velocity signal observed at the buoy from September 23 to October 7 (peaking at -0.4 m s^{-1} on September 26) would have arrived at 150°W exactly during Flupac TS II (October 19–25), assuming a typical westward propagation of 0.4 d^{-1} (Fig. 4) (Qiao and Weisberg, 1995). These observations were confirmed by ADCP measurements made onboard the R/V *Atalante* showing v in the upper 50 m starting near zero at the beginning of TS II, peaking to 0.5 m s^{-1} on October 22 and dropping to 0.3 m s^{-1} by the end of the time series (Le Borgne et al., 1995). Because southward meridional velocities are highly correlated with strong upwelling rates at the equator

(Weisberg and Qiao, 2000; Friedrichs and Hofmann, 2001), this is clear evidence that w was highly variable and probably peaked at relatively high values ($3\text{--}6 \text{ m d}^{-1}$) during Flupac TS II, despite the observation that upwelling fluxes were minimal during the previous month 2000 km to the west. The drift of the vessel from the equator to 0.5°S during the last 3 days of Flupac TS II (Le Borgne et al., 1995) is likely to have little effect on these conclusions, given typical spatial distributions of upwelling (Harrison, 1996). However, it is impossible to know exact daily patterns of w without a compact array of moored velocity profilers such as employed by Weisberg and Qiao (2000).

Therefore, Flupac TS II sampled a rare combination of physical forcings on upwelled nutrient fluxes. Despite strong and variable upwelling velocities, the highly depressed thermocline allowed for low variability in temperature and nutrient profiles. These observed physical conditions agree quite well with the nitrogen–iron model. Stations during Flupac Time Series II all plot along a line of roughly constant upwelled nitrate concentration, near $4.5 \mu\text{M}$ (Fig. 2a), and over a large range of upwelling velocities, from 1.3 to 3.6 m d^{-1} . It appears then that the high variability in new production measured during Flupac TS II resulted almost entirely from fluctuations in upwelling velocity.

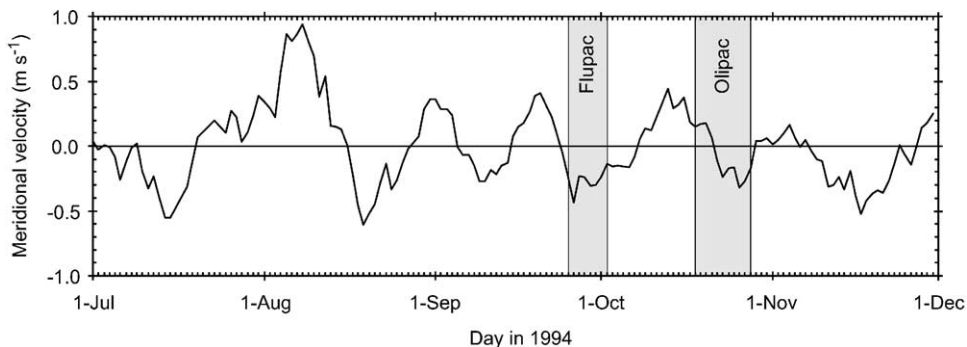


Fig. 4. Daily averaged meridional advection velocities (v) at 30 m depth on the TAO buoy on the equator at 140°W, showing a progression of passing TIWs with typical periods of 20–30 days. Southward (negative) velocities are strongly correlated with positive upwelling rates at the equator (Weisberg and Qiao, 2000; Friedrichs and Hofmann, 2001). Shaded regions indicate the portions of TIWs that would have passed 150°W during Flupac TS II (October 19–26) and during the sampling of Olipac stations between the equator and with 5°S (November 11–21), assuming a typical 0.4 d^{-1} westward propagation (Qiao and Weisberg, 1995).

3.1.3. *EqPac Time Series II and Survey II*

The second set of EqPac cruises occurred during normal (non-El Niño) cold-tongue conditions more similar to those of Zonal Flux yet also during the same season as Flupac (August to October) that is characterized by TIW activity. This combination resulted in these EqPac cruises observing a combination of forcing modes. As is typical of the season, a moderate-to-strong TIW was documented to have passed during Time Series II (Foley et al., 1997; Friedrichs and Hofmann, 2001), driving strong and highly variable upwelling velocities (Friedrichs and Hofmann, 2001). The nutricline (defined as the $7\ \mu\text{M}$ nitrate isopleth) was quite shallow, 50–70 m less deep than during Flupac. This resulted not only in higher nitrate concentrations but also enhanced the ability of two passing IGW to drive 20–30 m oscillations in nutricline depth (Friedrichs and Hofmann, 2001). Nitrate concentrations ranged from 6.5 to $11.5\ \mu\text{M}$ at 80 m and from 11 to $14\ \mu\text{M}$ at 120 m (P. Wheeler, <http://www1.who.edu/jgofs.html>). During EqPac Survey II a high-amplitude TIW passed (Foley et al., 1997), again driving large fluctuations in upwelling velocities with large spatial as well as temporal variability (Friedrichs and Hofmann, 2001). As a consequence of sampling across the equator during this period, nitrate concentrations from 3°N to 3°S ranged from 3.5 to $9\ \mu\text{M}$ at 80 m and from ~ 10 to $21\ \mu\text{M}$ at 120 m (Garside, 1996).

Comparison of a plot of NP vs. mixed-layer nitrate with modeled contours (Fig. 2b and c) paints nearly the same pattern of physical forcing as these independent observations. For TS II, points plot over a range of $[\text{NO}_3^-]_{\text{up}}$ values, 7– $11\ \mu\text{M}$, which match observed concentrations at upwelling depths quite well (Fig. 2b). Likewise, the range in upwelling velocities suggested by the model, $0.3\text{--}2.4\ \text{m d}^{-1}$, are reasonable daily averages during this period (Friedrichs and Hofmann, 2001). Within the upwelling region (3°N – 3°S) during Survey II, plotted points suggest $[\text{NO}_3^-]_{\text{up}}$ values of 6– $11\ \mu\text{M}$ that also fit with observations from likely upwelling depths (Fig. 2c). Model-inferred vertical velocities for Survey II of $0.1\text{--}1.8\ \text{m d}^{-1}$ are also not unreasonable. Therefore for EqPac Time Series II and the

equatorial section of Survey II (3°N – 3°S), the model suggests that the distinct relationship of NP to mixed-layer nitrate between stations was a consequence of large variability in upwelling velocity accompanied by more moderate changes in nutricline depth (Fig. 2b and c).

3.1.4. *EqPac Time Series I*

Occurring near the end of an El Niño, Time Series I captured the tail of a passing weak Kelvin wave (Foley et al., 1997) that allowed the thermocline to shoal appreciably just prior to sampling. Therefore, although mixed-layer nitrate concentrations were nearly the same during Time Series I as during Flupac or EqPac Survey I, nutricline depths ($7\ \mu\text{M}$ nitrate isopleth) were 10–30 m shallower than for either of the other cruises. This resulted in relatively higher upwelled nitrate concentrations, ranging from 3.5 to $6\ \mu\text{M}$ at 80 m and $10.5\text{--}13.5\ \mu\text{M}$ at 120 m (P. Wheeler, <http://www1.who.edu/jgofs.html>). These concentrations are considerably more variable than observed during Flupac, as might be expected from the potential of a shallower nutricline to be more affected by variability in upwelling. Meridional currents actually hint at the passage of a weak TIW (Foley et al., 1997), and a moderate fluctuations in w were likely (Friedrichs and Hofmann, 2001). These observations again agree with inferences from the coupled nitrogen–iron model. The scattered position on the model grid corresponds to $[\text{NO}_3^-]_{\text{up}}$ values of 4– $6\ \mu\text{M}$ and vertical velocities on the order of $1.2\text{--}2.0\ \text{m d}^{-1}$, and the lack of a relationship between NP and nitrate suggests that nutrient fluxes were forced by a balanced mixture of variability in w and in nutricline depth (Fig. 2b).

3.1.5. *EqPac Survey I, WEC88, WEC8803-B and other stations with low new production*

All values measured during EqPac Survey I lie near the model asymptote for minimum new production, as do stations from Survey II that are from $5\text{--}12^\circ\text{N}$ to $5\text{--}12^\circ\text{S}$ (Fig. 2c). For all of these stations the nutricline was typically rather deep and upwelling was likely to have been minimal given the strong El Niño and lack of

TIW activity during Survey I and the off-equator locations of these Survey II stations.

Observations from two other meridional transects to the region, WEC88 and WEC8803-B showed for the most part a similar pattern of rather minimal NP despite relatively high nitrate concentrations (Fig. 2d) (Dugdale et al., 1992; Peña et al., 1992). Only at the equator during WEC88 and within 2° of the equator during WEC8803-B did new production exceed $1.1 \text{ mmol N m}^{-2} \text{ d}^{-1}$. These cruises took place during “normal” conditions at the Pacific transitioned from 1986–1987 El Niño to the La Niña of the latter three quarters of 1988 (Barber, 1992). However, although these cruises sampled a relatively shallow nutricline, there was no evidence of TIW activity (as expected from the season) or any other reason to believe that upwelling rates were particularly vigorous. These observations match model predictions that such patterns of minimal new production are due to a deep nutricline or low w (or both) and that the atmospheric iron flux should largely determine new production values.

3.1.6. *Olipac*

This cruise sampled essentially the same meridional transect as WEC88, also near the end of an El Niño, yet the pattern of new production to nitrate was quite different than either WEC cruise. Although the equatorial nutricline was quite deep at the onset of Olipac, the cruise sampled the equator as a Kelvin wave forced the thermocline to shoal (Stoens et al., 1999, and TAO web site). At the same time the southward meridional signal of a TIW, associated with upwelling, is likely to have arrived at 150°W. How this TIW affected upwelling during Olipac is not as clear as for Flupac TS II, because the equator was only sampled 1 day (November 15). However, in general the strongest downwelling during a TIW is restricted to north of the equator, whereas TIW associated upwelling extends to 2°S (Harrison, 1996). Thus, it is most likely that upwelling was strong and variable within for Olipac stations within several degrees of the equator. Indeed, NP and mixed-layer nitrate data for these stations plot on model contours suggesting this very scenario. Interesting to note are three high NP values at very low mixed-layer

nitrate concentrations at stations far from the equator. Are these indicative of dust deposition events?

In general, observations at sea match quite well the inferences that can be made by comparing model results to patterns of new production and mixed-layer nitrate concentration. This close correspondence strongly suggests that the general model result is correct. Differences in the relationships of new production to nitrate inventory that were observed during Zonal Flux, Flupac and other cruises thus appear to be attributable to different modes of physical forcing between cruises.

3.2. *Implications for other iron-limited regions*

While conceived in the context of the equatorial Pacific, the conceptual framework used to construct the model is general to most iron-limited oceanic ecosystems. Thus general concepts derived from this model should be broadly applicable elsewhere. We made only one simplification not generally valid for other regions, that mixing is negligible relative to advection. By including mixing as a component of F_{X-up} , Eqs. (6) and (10) only change in that a new term is added to term A (Eq. (7)). This vertical mixing term is $BK_z \{ (N/Fe)_{OM} \cdot dFe/dz - dN/dz \}$. However, for most regions this term is likely to approach zero because near the nutricline the vertical dissolved iron gradient (dFe/dz) multiplied by $(N/Fe)_{OM}$ should roughly equal the nitrate gradient (dN/dz) in iron-limited waters. Indeed, comparing nitrate and dissolved iron profiles from the global iron dataset (Johnson et al., 1997, Appendix A) suggests that nitrate and iron gradients do match near the bottom of the mixed layer. However, at stations where atmospheric iron deposition appeared important, $[Fe]$ often increases in the upper 50 m, and at stations where $[Fe]$ was below the detection limit (i.e. EqPac TS I & II) it is not possible to confirm the validity of the assumption that $(N/Fe)_{OM} \cdot dFe/dz \approx dN/dz$.

For regions where horizontal advection and mixing are important (i.e. off the equator), one can imagine that the box is simply turned on its side. Broadly speaking, F_{X-up} can be considered as any

advective (and mixing) supply flux into the box, F_{X-in} . However, estimating the water volume flux and its flux-weighted average nitrate concentration certainly would be more complicated when considering three-dimensional advection. Furthermore, when waters enter a study site by horizontal advection from waters already at the surface, estimates of the nitrate-to-iron ratio in source waters would need to take into account atmospheric iron inputs and preferential biological uptake of iron (relative to nitrate) in the upstream box with each timestep. Despite these complications, conclusions from this simple model should be applicable to a broad range of iron-limited, HNLC regions. However, light limitation will regulate when this model is applicable in the north Pacific and the Southern Ocean. On the other hand, even in many regions where nitrogen is considered limiting (i.e. oligotrophic gyres), the model provides the useful concept that atmospheric iron supply places an upper bound on new production (i.e. $NP < A$) (Eqs. (6–9)).

In iron-limited systems, observed relationships between new production and mixed-layer nitrate concentrations depend on which driver of iron supply (w or $[NO_3^-]_{up}$) is most variable within that set of observations. This is perhaps the most important conclusion from this paper. It means that the observed variability in the slope and shape of new production to nitrate relationships (Aufdenkampe et al., 2002) should in fact be expected. In the nitrogen-limited oligotrophic gyres, episodic atmospheric depositional events could drive changes in new production while maintaining negligible mixed-layer nitrate concentrations, possibly by promoting nitrogen fixation (Fig. 5a). Likewise, large dust events could drive a weakly HNLC ecosystem into nitrogen limitation. In strongly HNLC regions, a set of observations made during consistently low advection rates might exhibit nearly constant NP as a function of mixed-layer nitrate, even when sampling over a wide range of nutricline depths (Fig. 5b). If a transition into a large dust event were sampled in

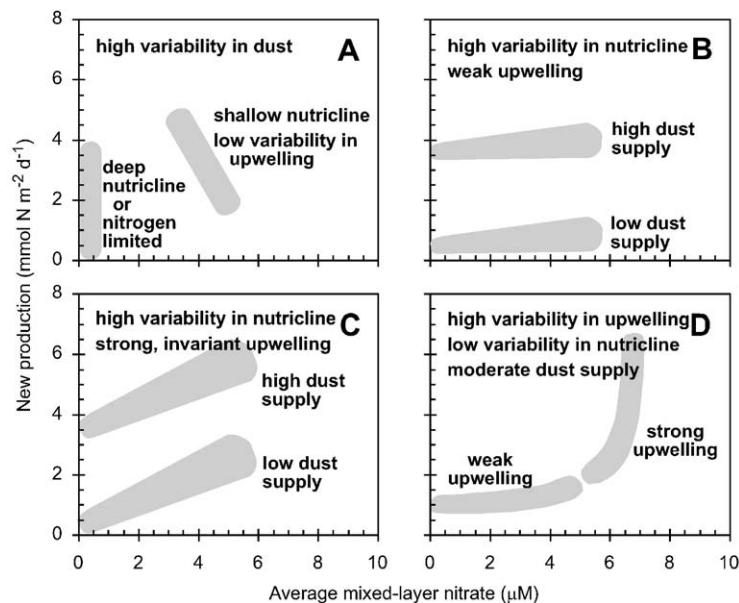


Fig. 5. Patterns in areal new production as a function of mixed-layer nitrate concentrations that are possible for a set of stations under different conditions. Plots compare patterns that might result from variability in total iron supply being dominated by variability in (A) dust supply, (B) and (C) nutrient depth, and (D) upwelling advection rates (or horizontal advection, see text). (B) and (C) differ only in the relative magnitude of advection rates. These conditions will vary spatially as well as temporally. For example, the scenario of variability depicted in B is most likely observed by sampling across hydrographic regions.

such a region, a negative correlation between NP and nitrate might be observed (Fig. 5a). At other times of strong but invariant advection, a strong positive correlation could appear (Fig. 5c). Where advection fluctuations are much greater than other variability, a curved relationship might exist, appearing as a threshold nitrate concentration requirement for NP stimulation (e.g. Dugdale et al., 1990; McCarthy et al., 1996) (Fig. 5d). A broad scatter of NP and nitrate values that shows no relationship might be observed where iron supplies are modulated by two or more of these modes of variability. Lastly, unlike the equatorial Pacific, atmospheric iron fluxes generally exceed upwelling fluxes in most regions of the world (Fung et al., 2000). Therefore, the high dust-supply scenarios depicted in these plots may be more common in the world's iron-limited oceans.

The three primary modes of forcing on iron supply—vertical advection rates, concentrations at advection sources (or nutricline depth), and atmospheric deposition—are each characterized by different timescales and spatial patterns. On the shortest time scales (hours to days), fluctuations in vertical velocity dominate for a given location (Flupac TS II and EqPac TS II, Fig. 2a and b). Episodic deposition events also might trigger short-scale variability (days to weeks), but these events are relatively rare in iron-limited regions. On longer time scales (weeks to years), variability in nutricline depth is most important (EqPac TS I relative to TS II, Fig. 2b), yet cruises sampling a transect through different hydrographic regions could also observe this type of variability (Zonal Flux and EqPac Survey II, Fig. 2a and c). Therefore it is not at all surprising that multiple regression analysis of new production in the tropical Pacific revealed very different patterns of NP-to-nitrate variability within individual cruises relative to the relationship between cruises (Aufdenkampe et al., 2002).

4. Conclusions

The relative difficulty of acquiring data in ocean systems has long inspired oceanographers to employ simple models and clever proxies. This

study extends that tradition by building a simple one-box model from mass-balance concepts, in order to explain how nitrate might serve as a proxy for iron (Eq. (5)) and new production (Eqs. (6–10)) in HNLC and other iron-limited regions such as the equatorial Pacific. The most important result from model equations is that HOW the iron flux varies between a set of stations is the critical factor in determining the observed relationship between new production and mixed-layer nitrate concentrations. Variability in upwelling velocities, nutricline depth, atmospheric deposition or any combination of the three each results in characteristic patterns in NP and nitrate. Plots of these patterns from each of six cruises in the equatorial Pacific (Fig. 2) imply variability in physical forcing that agrees well with independent observations of physical conditions during each cruise. The Zonal Flux and Flupac TS II cruises serve as excellent examples of end-members of these processes. Therefore, the simple model appears to offer a realistic, mechanistic understanding of how physical forcing in the equatorial Pacific modulates new production to nitrate relationships through iron.

As with most natural systems, the equatorial Pacific Ocean reveals increasing levels of complexity the further it is studied. The early paradigm of relative biological stability is giving way to the understanding that a number of physical processes can drive substantial variability in chlorophyll, primary, new and export production (e.g. Barber et al., 1996; Chavez et al., 1999; Dunne et al., 2000; Friedrichs and Hofmann, 2001). Understanding the controls on new production relative to unused nitrate (and by extension carbon dioxide) that is exported from HNLC regions is especially important to efforts at modeling the global carbon cycle. Recent multivariate statistical results (Aufdenkampe et al., 2001, 2002) have elucidated a number of proxies for new production and offer potential to estimate its variability from remotely acquired data. Despite demonstrating substantial uniformity in patterns of NP to nitrate within cruises, these patterns showed real differences between cruises. The simple mechanistic model developed here explains those differences, offering insights into how physical and biological processes are linked within the equatorial Pacific.

Acknowledgements

We thank M.A.M. Friedrichs, W. Gentleman, W.S. Kessler, E. Laws, M. Rodier and one anonymous reviewer for many helpful comments and J.I. Hedges and J.E. Richey for their encouragement and support. We also thank R. Le Borgne for his editorial handling of this manuscript. This work was funded by NSF grant OCE 9504202. This is US JGOFS contribution No. 784.

References

- Archer, D.E., Peltzer, E.T., Kirchman, D.L., 1997. A timescale for dissolved organic carbon production in equatorial Pacific surface waters. *Global Biogeochemical Cycles* 11, 435–452.
- Aufdenkampe, A.K., McCarthy, J.J., Rodier, M., Navarette, C., Dunne, J.P., Murray, J.W., 2001. Estimation of new production in the tropical Pacific. *Global Biogeochemical Cycles* 15, 101–113.
- Aufdenkampe, A.K., McCarthy, J.J., Navarette, C., Rodier, M., Dunne, J., Murray, J.W., 2002. Biogeochemical controls on new production in the tropical Pacific. *Deep-Sea Research II* 49, 2619–2648.
- Barbeau, K., Moffett, J.W., 2000. Laboratory and field studies of colloidal iron oxide dissolution as mediated by phagotrophy and photolysis. *Limnology and Oceanography* 45, 827–835.
- Barbeau, K., Moffett, J.W., Caron, D.A., Croot, P.L., Erdner, D.L., 1996. Role of protozoan grazing in relieving iron limitation of phytoplankton. *Nature* 380, 61–64.
- Barber, R.T., 1992. Introduction to the WEC88 Cruise: an investigation into why the equator is not greener. *Journal of Geophysical Research* 97, 609–610.
- Barber, R.T., Sanderson, M.P., Lindley, S.T., Chai, F., Newton, J., Trees, C.C., Foley, D.G., Chavez, F.P., 1996. Primary productivity and its regulation in the equatorial Pacific during and following the 1991–1992 El Niño. *Deep-Sea Research II* 43, 933–969.
- Behrenfeld, M.J., Bale, A.J., Kolber, Z.S., Aiken, J., Falkowski, P.G., 1996. Confirmation of iron limitation of phytoplankton photosynthesis in the equatorial Pacific Ocean. *Nature* 383, 508–511.
- Brady, E.C., Bryden, H.L., 1987. Estimating vertical velocity on the Equator. *Oceanologica Acta* HS, 33–37.
- Carpenter, E.J., Capone, D.G., 1992. Nitrogen fixation in *Trichodesmium* blooms. In: Carpenter, E.J., Capone, D.G., Rueter, J.G. (Eds.), *Marine Pelagic Cyanobacteria*. Kluwer, Dordrecht, pp. 211–217.
- Carr, M.-E., Lewis, M.R., Kelly, D., Jones, B., 1995. A physical estimate of new production in the equatorial Pacific along 150°W. *Limnology and Oceanography* 40, 138–147.
- Chavez, F.P., Strutton, P.G., Friederich, G.E., Feely, R.A., Feldman, G.C., Foley, D.G., McPhaden, M.J., 1999. Biological and chemical response of the equatorial Pacific to the 1997–1998 El Niño. *Science* 286, 2126–2131.
- Coale, K.H., Fitzwater, S.E., Gordon, R.M., Johnson, K.S., Barber, R.T., 1996. Control of community growth and export production by upwelled iron in the equatorial Pacific. *Nature* 379, 621–624.
- Duce, R.A., Tindale, N.W., 1991. Atmospheric transport of iron and its deposition in the ocean. *Limnology and Oceanography* 36, 1715–1726.
- Dugdale, R.C., Goering, J.J., 1967. Uptake of new and regenerated forms of nitrogen in primary productivity. *Limnology and Oceanography* 12, 196–206.
- Dugdale, R.C., Wilkerson, F.P., 1992. Nutrient limitation of new production in the sea. In: Falkowski, P.G., Woodhead, A.D. (Eds.), *Primary Productivity and Biogeochemical Cycles in the Sea*. Plenum Press, New York, pp. 107–122.
- Dugdale, R.C., Wilkerson, F.P., Morel, A., 1990. Realization of new production in coastal upwelling areas: a means to compare relative performance. *Limnology and Oceanography* 35, 822–829.
- Dugdale, R.C., Wilkerson, F.P., Barber, R.T., Chavez, F.P., 1992. Estimating new production in the equatorial Pacific Ocean at 150°W. *Journal of Geophysical Research* 97, 681–686.
- Dunne, J.P., Murray, J.W., Rodier, M., Hansell, D.A., 2000. Export production in the western and central equatorial Pacific: zonal and temporal variability. *Deep-Sea Research I* 47, 901–936.
- Eldin, G., Rodier, M., Radenac, M.-H., 1997. Physical and nutrient variability in the upper equatorial Pacific associated with westerly wind forcing and wave activity in October 1994. *Deep-Sea Research II* 44, 1783–1800.
- Eppley, R.W., Peterson, B.J., 1979. Particulate organic matter flux and planktonic new production in the deep ocean. *Nature* 282, 677–680.
- Fitzwater, S.E., Coale, K.H., Gordon, R.M., Johnson, K.S., Ondrusek, M.E., 1996. Iron deficiency and phytoplankton growth in the equatorial Pacific. *Deep-Sea Research II* 43, 995–1015.
- Foley, D.G., Dickey, T.D., McPhaden, M.J., Bidigare, R.R., Lewis, M.R., Barber, R.T., Lindley, S.T., Garside, C., Manov, D.V., McNeil, J.D., 1997. Longwaves and primary productivity variations in the equatorial Pacific at 0°, 140°W. *Deep-Sea Research II* 44, 1801–1826.
- Friedrichs, M.A.M., Hofmann, E.E., 2001. Physical controls of biological processes in the central equatorial Pacific Ocean. *Deep-Sea Research II* 48, 1023–1069.
- Fung, I.Y., Meyn, S.K., Tegen, I., Doney, S.C., John, J.G., Bishop, J.K.B., 2000. Iron supply and demand in the upper ocean. *Global Biogeochemical Cycles* 14, 281–295.
- Garside, C., 1996. Nutrient data for EqPac Surveys I and II. US JGOFS Web Page (<http://www1.whoi.edu/jgofs.html>).

- Gordon, R.M., Coale, K.H., Johnson, K.S., 1997. Iron distributions in the equatorial Pacific: implications for new production. *Limnology and Oceanography* 43, 419–431.
- Halpern, D., Freitag, H.P., 1987. Vertical motion in the upper ocean of the equatorial eastern Pacific. *Oceanologica Acta HS*, 19–26.
- Hansell, D.A., Bates, N.R., Carlson, C.A., 1997a. Predominance of vertical loss of carbon from surface waters of the equatorial Pacific Ocean. *Nature* 386, 59–61.
- Hansell, D.A., Carlson, C.A., Bates, N.R., Poisson, A., 1997b. Horizontal and vertical removal of organic carbon in the equatorial Pacific Ocean: a mass balance assessment. *Deep-Sea Research II* 44, 2115–2130.
- Harrison, D.E., 1996. Vertical velocity in the central tropical Pacific: a circulation model perspective for JGOFS. *Deep-Sea Research II* 43, 687–705.
- Johnson, K.S., Coale, K.H., Elrod, V.A., Tindale, N.W., 1994. Iron photochemistry in seawater from the Equatorial Pacific. *Marine Chemistry* 46, 319–334.
- Johnson, K.S., Gordon, R.M., Coale, K.H., 1997. What controls dissolved iron concentrations in the world ocean? *Marine Chemistry* 57, 137–161.
- Kessler, W.S., McPhaden, M.J., 1995. The 1991–1993 El Niño in the central Pacific. *Deep-Sea Research II* 42, 295–333.
- Landry, M.R., Barber, R.T., Bidigare, R.R., Chai, F., Coale, K.H., Dam, H.G., Lewis, M.R., Lindley, S.T., McCarthy, J.J., Roman, M.R., Stoecker, D.K., Verity, P.G., White, J.R., 1997. Iron and grazing constraints on primary production in the central equatorial Pacific: an EqPac synthesis. *Limnology and Oceanography* 42, 405–418.
- Le Borgne, R., Brunet, C., Eldin, G., Radenac, M.-H., Rodier, M., 1995. Campagne océanographique FLUPAC à bord du N. O. L'ATALANTE (23 septembre au 29 octobre 1994). Recueil de données. Tome 1: météo, courantologie, hydrologie, données de surface, ORSTOM-Nouméa.
- Leonard, C.L., McClain, C.R., Murtugudde, R., Hofmann, E.E., Harding Jr., L.W., 1999. An iron-based ecosystem model of the central equatorial Pacific. *Journal of Geophysical Research* 104, 1325–1341.
- Libby, P.S., Wheeler, P.A., 1997. Particulate and dissolved organic nitrogen in the central and eastern equatorial Pacific. *Deep-Sea Research I* 44, 345–361.
- Loukos, H., Frost, B., Harrison, D.E., Murray, J.W., 1997. An ecosystem model with iron limitation of primary production in the equatorial Pacific at 140°W. *Deep-Sea Research II* 44, 2221–2249.
- Maranger, R., Bird, D.F., Price, N.M., 1998. Iron acquisition by photosynthetic marine phytoplankton from ingested bacteria. *Nature* 396, 248–251.
- Martin, J.H., Fitzwater, S.E., 1988. Iron deficiency limits phytoplankton growth in the north-east Pacific subarctic. *Nature* 331, 341–343.
- Martin, J.H., Coale, K.H., Johnson, K.S., Fitzwater, S.E., Gordon, R.M., Tanner, S.J., Hunter, C.N., Elrod, V.A., Nowiki, J.L., Coley, T.L., Barber, R.T., Lindley, S.T., Watson, A.J., Van Scoy, K., Law, C.S., Liddicoat, M.I., Ling, R., Stanton, T., Stockel, J., Collins, C., Anderson, A., Bidigare, R.R., Ondrusek, M.E., Latasa, M., Millero, F.J., Lee, K., Yao, W., Zhang, J.Z., Friederich, G., Sakamoto, C., Chavez, F.P., Buck, K., Kolber, Z., Greene, R., Falkowski, P.G., Chisholm, S.W., Hoge, F., Swift, R., Yungel, J., Turner, S., Nightingale, P., Hatton, A., Liss, P., Tindale, N.W., 1994. Testing the iron hypothesis in ecosystems of the equatorial Pacific Ocean. *Nature* 371, 123–129.
- McCarthy, J.J., Garside, C., Nevins, J.L., Barber, R.T., 1996. New production along 140°W in the equatorial Pacific during and following the 1992 El Niño event. *Deep-Sea Research II* 43, 1065–1093.
- McCarthy, J.J., Garside, C., Nevins, J.L., 1999. Nitrogen dynamics during the Arabian Sea Northeast Monsoon. *Deep-Sea Research II* 46, 1623–1664.
- Murray, J.W., Young, J., Newton, J., Dunne, J.P., Chapin, T., Paul, B., McCarthy, J.J., 1996. Export flux of particulate organic carbon from the central equatorial Pacific determined using a combined drifting trap—²³⁴Th approach. *Deep-Sea Research II* 43, 1095–1132.
- Navarette, C., 1998. Dynamique du phytoplancton en océan équatorial: mesures cytométriques et mesures isotopiques durant la campagne FluPac, en octobre 1994 dans la partie ouest du pacifique, Doctoral Dissertation, Université Paris VI, Paris.
- Peña, M.A., Harrison, W.G., Lewis, M.R., 1992. New production in the central equatorial Pacific. *Marine Ecology Progress Series* 80, 265–274.
- Platt, T., Harrison, W.G., 1985. Biogenic fluxes of carbon and oxygen in the ocean. *Nature* 318, 55–58.
- Qiao, L., Weisberg, R.H., 1995. Tropical instability waves kinematics: observations from the tropical instability wave experiment. *Journal of Geophysical Research* 100, 8677–8694.
- Raimbault, P., Slawyk, G., Boudjellal, B., Coatanoan, C., Conan, P., Coste, B., Garcia, N., Moutin, T., Pujon-Pay, M., 1999. Carbon and nitrogen uptake and export in the equatorial Pacific at 150°W: evidence of an efficient regenerated production cycle. *Journal of Geophysical Research* 104, 3341–3356.
- Rodier, M., Le Borgne, R., 1997. Export flux of particles at the equator in the western and central Pacific Ocean. *Deep-Sea Research II* 44, 2085–2113.
- Rodier, M., Eldin, G., Le Borgne, R., 2000. The western boundary of the equatorial Pacific upwelling: some consequences of climatic variability on hydrological and planktonic properties. *Journal of Oceanography* 56, 463–471.
- Spokes, L.J., Jickells, T.D., Lim, B., 1994. Solubilisation of aerosol trace metals by cloud processing: a laboratory study. *Geochimica et Cosmochimica Acta* 58, 3281–3287.
- Stoens, A., Menkès, C., Radenac, M.-H., Dandonneau, Y., Grima, N., Eldin, G., Mémerly, L., Navarette, C., André, J.-M., Moutin, T., Raimbault, P., 1999. The coupled physical-new production system in the equatorial Pacific during the 1992–1995 El Niño. *Journal of Geophysical Research* 104, 3323–3339.

- Sunda, W.G., 1997. Control of dissolved iron concentrations in the world ocean: a comment. *Marine Chemistry* 57, 169–172.
- Sunda, W.G., Huntsman, S.A., 1995. Iron uptake and growth limitation in oceanic and coastal phytoplankton. *Marine Chemistry* 50, 189–206.
- Tegen, I., Miller, R., 1998. A general circulation model study on the interannual variability of soil dust aerosol. *Journal of Geophysical Research* 103, 25975–925995.
- Toggweiler, J.R., Carson, S., 1995. What are upwelling systems contributing to the ocean's carbon and nutrient budgets? In: Summerhayes, C.P., Emeis, K.-C., Angel, M.V., Smith, R.L., Zeitzschel, B. (Eds.), *Upwelling in the Ocean; Modern Processes and Ancient Records*. Wiley, Chichester, UK, pp. 337–360.
- Weisberg, R.H., Qiao, L., 2000. Equatorial upwelling in the central Pacific estimated from moored velocity profilers. *Journal of Physical Oceanography* 30, 105–124.
- Wilkerson, F.P., Dugdale, R.C., 1992. Measurements of nitrogen productivity in the equatorial Pacific. *Journal of Geophysical Research* 97, 669–679.
- Wunsch, C., Gill, A.E., 1976. Observations of equatorially trapped waves in Pacific sea level variations. *Deep-Sea Research I* 23, 371–390.
- Zhang, J., Quay, P.D., 1997. The total organic carbon export rate based on DIC and DIC¹³ budgets in the equatorial Pacific Ocean. *Deep-Sea Research II* 44, 2163–2190.
- Zhu, X., Prospero, J.M., Millero, F.J., 1997. Diel variability of soluble Fe(II) and soluble total Fe in North African dust in the trade winds at Barbados. *Journal of Geophysical Research* 102, 21297–21305.
- Zhuang, G., Yi, X., Wallace, G.T., 1995. Iron (II) in rainwater, snow, and surface seawater from a coastal environment. *Marine Chemistry* 50, 41–50.